

TIME-DEPENDENT STOCHASTIC ACCELERATION MODEL FOR THE FERMI BUBBLES

KENTO SASAKI, KATSUAKI ASANO AND TOSHIO TERASAWA

Institute for Cosmic Ray Research, The University of Tokyo, 5-1-5 Kashiwanoha, Kashiwa, Chiba 277-8582, Japan
Draft version March 24, 2022

ABSTRACT

We study stochastic acceleration models for the Fermi bubbles. Turbulence is excited just behind the shock front via Kelvin–Helmholtz, Rayleigh–Taylor, or Richtmyer–Meshkov instabilities, and plasma particles are continuously accelerated by the interaction with the turbulence. The turbulence gradually decays as it goes away from the shock fronts. Adopting a phenomenological model for the stochastic acceleration, we explicitly solve the temporal evolution of the particle energy distribution in the turbulence. Our results show that the spatial distribution of high-energy particles is different from those for a steady solution. We also show that the contribution of electrons that escaped from the acceleration regions significantly softens the photon spectrum. The photon spectrum and surface brightness profile are reproduced by our models. If the escape efficiency is very high, the radio flux from the escaped low-energy electrons can be comparable to that of the WMAP haze. We also demonstrate hadronic models with the stochastic acceleration, but they are unlikely in the viewpoint of the energy budget.

Subject headings: acceleration of particles — cosmic rays — gamma rays: theory — radiation mechanisms:

1. INTRODUCTION

Gamma-ray data of the *Fermi* Large Area Telescope (LAT) reveal bilobal giant bubbles extending up to $\sim 50^\circ$ above and below the Galactic disk, called the “Fermi Bubbles (FBs)” (Su et al. 2010; Su & Finkbeiner 2012; Ackermann et al. 2014; Yang et al. 2014). There the microwave bubbles also exists in the same region, the WMAP haze (Finkbeiner 2004; Dobler & Finkbeiner 2008). These huge structures may suggest past large-scaled activities in the Galactic Center, such as active galactic nucleus (AGN) jet activity (e.g. Guo & Mathews 2012; Yang et al. 2012), non-relativistic outflow from the nucleus (e.g. Zubovas, King & Nayakshin 2011; Zubovas & Nayakshin 2012; Mou et al. 2014), or wind driven by supernovae (e.g. Crocker 2012; Lacki 2014). The gamma-ray spectra of the FBs are harder than the ambient diffuse spectrum of the Galactic halo, and the surface brightness profiles show a sharp rise at the bubble edges. The intensity inside the FBs is almost constant, which requires inhomogeneous gamma-ray emissivity inside the FBs. If the volume emissivity is constant, the surface brightness should show a bump-like profile with gradually rising edges as a result of the projection effect (Mertsch & Sarkar 2011). On the other hand, a localized emissivity at the shock fronts should yield limb-brightened profiles. Significantly thick shells are therefore preferable for the emission regions.

As emission mechanisms, hadronic (Crocker and Aharonian 2011; Fujita, Ohira & Yamazaki 2013; Cheng et al. 2015a) and leptonic (Cheng et al. 2011, 2014, 2015b; Mertsch & Sarkar 2011) models were proposed. In hadronic models, shock-accelerated protons produce pions via pp -collision, and gamma-rays are emitted from π^0 -decay. The present Mach number of the shocks

is not so large (Tahara et al. 2015) that the direct shock acceleration may not be effective. High-energy protons that were shock-accelerated past early-stages may still be confined in the FBs. Such protons widely distributed in the downstream may be responsible for the gamma-ray emission (Fujita, Ohira & Yamazaki 2013, 2014). In leptonic models, high-energy electrons emit gamma-rays via inverse Compton (IC) scattering. The short cooling timescale for electrons requires continuous acceleration in the downstream to secure a large volume of the emission region. The second order Fermi acceleration is the most promising candidate for such an acceleration mechanism. Electrons may be continuously accelerated by scattering with turbulences in the FBs. The stochastic acceleration is a candidate of the particle acceleration mechanisms in supernova remnants (Fan, Liu & Fryer 2010), lobes of radio galaxies (Hardcastle et al. 2009; O’Sullivan, Reville & Taylor 2009), blazars (Asano et al. 2014; Asano & Hayashida 2015; Kakuwa et al. 2015), and gamma-ray bursts (Asano & Terasawa 2009). Mertsch & Sarkar (2011, hereafter MS11) succeeded in reproducing the gamma-ray spectrum and surface brightness profile with such a stochastic acceleration model, taking into account the gradual decay of the turbulences in the downstream. Cheng et al. (2014, 2015b) also considered the stochastic acceleration in certain localized regions.

In this paper, we revisit the stochastic acceleration model for the FBs focusing on the effects of the time-dependence and escape from the acceleration regions. We phenomenologically simulate the acceleration and photon emission of the electrons advected away from the shock front with evolving acceleration efficiency. We also show that the emission from the escaped electrons from the acceleration regions is important. Note that MS11 adopted steady solutions for the electron energy distribution, while the diffusion coefficient in the momentum space is assumed to decay with time. In addition, the

steady solutions accompany electron escape, but the escaped electrons are neglected in MS11. The model in Cheng et al. (2015b) is a different type of model, in which the shock fronts do not play an important role. Our goal is to find the best phenomenological description of the diffusion coefficient evolving in the downstream region rather than probe details of the acceleration mechanism. The validity of the obtained requirements for particle acceleration will be testified by future studies.

The radio emission from the WMAP haze is hard to reconcile both the hadronic and leptonic models. The amount of the secondary positrons/electrons generated from π^\pm is insufficient to reproduce the WMAP haze by synchrotron radiation. Another leptonic component is required to reproduce the WMAP haze in the hadronic models (Fujita, Ohira & Yamazaki 2014; Cheng et al. 2015a). Even for the leptonic models, a stronger magnetic field than the typical galactic value ($B \sim 4\mu\text{G}$) is needed in MS11. We therefore try to search a condition to reproduce both the FBs and WMAP haze in our picture.

In §2, we present our model assumption and computing method. The results are summarized in Sections 3 and 4 for leptonic and hadronic models, respectively. Section 5 provides a summary and discussion.

2. MODEL AND METHOD

There may exist a shock front, propagating outward, near the edge of the FBs. In the downstream of the shock, plasma turbulences are probably excited via Kelvin–Helmholtz instability (Guo & Mathews 2012), Rayleigh–Taylor instability (Mueller et al. 1991; Baumgartner & Breitschwerdt 2013; Yang & Liu 2013), or Richtmyer–Meshkov instability (Inoue, Yamazaki, & Inutsuka 2009). In our model, as assumed in MS11, electrons/protons are stochastically accelerated by scattering with the turbulences. We primarily consider the electron acceleration model, but hadronic models, where protons are accelerated by turbulences, are also discussed in this paper. The particle escape from the acceleration process is a nontrivial problem. When the diffusion length scale becomes larger than the size of the FB, particles can escape from the FBs (Ohira, Murase & Yamazaki 2011). The large size of the FBs and small spatial diffusion coefficient implied from the efficient scattering in our model suggest that we can neglect the escape of the particles from the FBs. Actually, the one-dimensional (1D) models taking into account the diffusion of particles in Fujita, Ohira & Yamazaki (2013, 2014) almost confine the accelerated particles within the FBs. As will be shown below, however, the continuous acceleration models without the escape effect are difficult to reconcile with the observed spectra. MS11 considered the steady-state model with the escape effect. Similarly to their model, we assume patchy disturbed regions (hereafter DRs) with a scale of L (see Figure 1), which may correspond to the size of the inhomogeneity in the upstream fluid for the Richtmyer–Meshkov instability model. In our model, particles are accelerated by the turbulences in the DRs, and escape with a certain probability. The DRs are advected away from the shock front with a speed of v_{sh} as depicted in Figure 1.

In this case, the evolution of the particle energy dis-

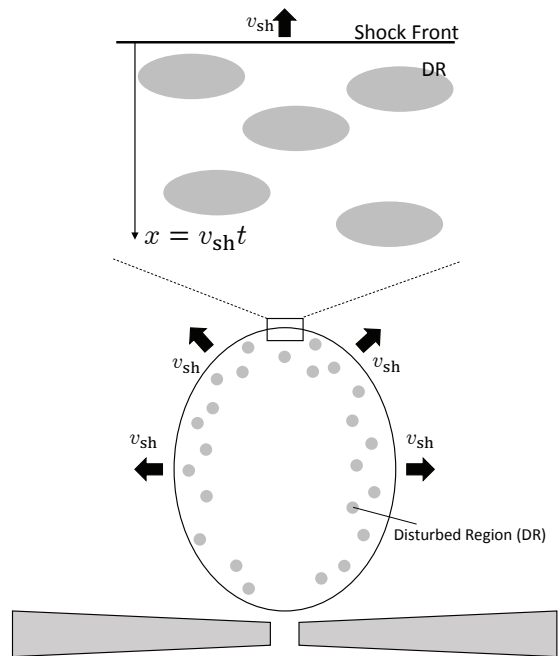


FIG. 1.— Schematic picture of our model. Plasma particles in the disturbed region, whose typical size is L , are accelerated by turbulences. The distance from the shock front x and elapsed time t are connected as $x = v_{\text{sh}}t$.

tribution in the DR rest frame is written by the Fokker–Planck equation (see, e.g. Stawarz & Petrosian 2008),

$$\frac{\partial n}{\partial t} - \frac{\partial}{\partial p} \left(p^2 D_{pp} \frac{\partial n}{\partial p} \right) + \frac{n}{t_{\text{esc}}} + \frac{\partial}{\partial p} \left(\frac{dp}{dt} n \right) - Q_{\text{inj}} = 0 \quad (1)$$

where the second–fifth terms represent the energy change via the stochastic process, the escape from the DRs, the cooling by the synchrotron and IC radiation, and the particle injection, respectively. The particle density $n(p, t)$ is the average density, while the actual density is higher according to the inverse of the filling factor of the DRs. At the present stage, the filling factor is unpredictable, depending on the mechanism of the hydrodynamical instability or the density-inhomogeneity formation in the upstream. We neglect the volume change of the DR so that the adiabatic cooling term is omitted.

The properties of the turbulences responsible for the particle acceleration are highly uncertain; the initial ratio of the average Alfvén speed to the turbulent velocity, the dominant wave mode (Alfvén or acoustic etc., see, e.g. Cho & Lazarian 2006), and the range of the wavenumber. The resonant interaction between particles and the Alfvén wave (see, e.g. Blandford & Eichler 1987; Stawarz & Petrosian 2008) is a possible candidate for the electron acceleration mechanism. Alternatively, fast mode waves have been frequently considered to be the scatterers of electrons (e.g. Liu et al. 2006; Fan, Liu & Fryer 2010), though the cut-off length scale due to wave damping depends on the unknown initial condition. Moreover, the recent simulations (Lynn et al. 2014) showed that slow mode waves can be dominant accelerators as well, even when the wave-particle resonance condition is not satisfied. It may be difficult to specify the acceleration process in the FBs from the observations at the present stage. Even if we

successfully reproduce the FBs by a detailed model of the temporal evolution motivated by a specific physical mechanism, this may not necessarily mean the validity of the supposed mechanism. Therefore, we first find a phenomenological evolution of the acceleration process to reproduce the FBs. Then, the required evolution should be examined by future plasma simulations.

We treat only ultra-relativistic particles, then the momentum diffusion coefficient can be phenomenologically described as

$$D_{pp}(p, t) \equiv \frac{2}{3} \beta_W^2 D p^q, \quad (2)$$

irrespective of the wave mode (e.g. Blandford & Eichler 1987; Cho & Lazarian 2006). Here, $v_W = \beta_W c$ is the effective wave velocity, which may correspond to the sound velocity or the Alfvén velocity. The factor β_W^2 implies that the average energy gain per scattering is proportional to $\beta_W^2 p$. The coefficient D is defined with the mean free path $l_{\text{mfp}}(p)$ as $D \equiv p^{2-q} c / l_{\text{mfp}}$. In this paper, we consider a case of $q = 2$ only (hard sphere approximation) to produce significantly soft gamma-ray spectra for the sub-GeV region to be consistent with the observations. In this case, l_{mfp} and the acceleration timescale $\sim p^2 / D_{pp}$ become energy-independent. The same assumption $q = 2$ as that in MS11 may be consistent with the nonresonant scattering by acoustic modes in turbulence with a typical eddy size (Ptuskin 1988; Cho & Lazarian 2006; Lynn et al. 2014). Even for resonant scattering by the Alfvén wave, the wavenumber spectrum $\propto k^{-2}$ in simulations of freely decaying magnetohydrodynamic turbulence (Christensson, Hindmarsh & Brandenburg 2001; Brandenburg, Kahniashvili & Tevzadze 2015) may support the index $q = 2$.

The spatial diffusion coefficient $D_{xx} \sim (1/3) c l_{\text{mfp}}$ is also described with D as

$$D_{xx}(t) \equiv \frac{c^2}{3D}. \quad (3)$$

While MS11 adopted a model with decaying fast magnetosonic waves based on Fan, Liu & Fryer (2010), we simply assume a power-law temporal evolution for D . Setting $t = 0$ at the shock front, we express

$$D(t) \equiv D_0 \left(1 + \frac{t}{t_0}\right)^{-\alpha}, \quad (4)$$

where the typical crossing timescale $t_0 \equiv L/v_{\text{sh}}$ is introduced to avoid divergence at $t = 0$. The escape timescale from the DRs is written as $t_{\text{esc}} \equiv L^2/D_{xx}$.

The decay index α is a free parameter in this paper. However, as will be shown, $\alpha \sim 1$ seems favorable for the FBs. Interestingly, three-dimensional (3D) numerical simulations of freely decaying magnetohydrodynamic turbulences show inverse cascades, in which the energy density of the turbulence decays ($U \propto t^{-0.7} t^{-1.1}$) with a wavenumber spectrum $\propto k^{-2}$, while the eddy size grows ($l_{\text{edd}} \propto t^{0.4} t^{0.5}$) (Christensson, Hindmarsh & Brandenburg 2001; Brandenburg, Kahniashvili & Tevzadze 2015). For both the resonant scattering with the Alfvén wave (Blandford & Eichler 1987) and the nonresonant scattering with acoustic waves (Lynn et al. 2014), $D \propto U/l_{\text{edd}}$ so that $\alpha \sim 1$ may be acceptable. In any case,

note that our purpose in this paper is to constrain the phenomenological parameters such as D_0 rather than determine the turbulence decay process and the microscopic mechanism of the electron acceleration.

The synchrotron and IC coolings for electrons are numerically treated with the standard method including the Klein–Nishina effect. The magnetic field is assumed as $B_0 = 4\mu\text{G}$ for the entire region. The model of the interstellar radiation field is taken from the GALPROP code¹ (v54, Vladimirov et al. 2011, and references therein), in which the model of Porter & Strong (2005) is adopted. We do not take into account the inhomogeneity of the radiation field, but adopt a representative field at $R = 2$ kpc and $z = 5$ kpc in the Galactocentric coordinate as shown in Figure 2 (the energy density $U_{\text{ph}} = 1.5 \times 10^{-12} \text{ erg cm}^{-3}$). We neglect the cooling effect for protons.

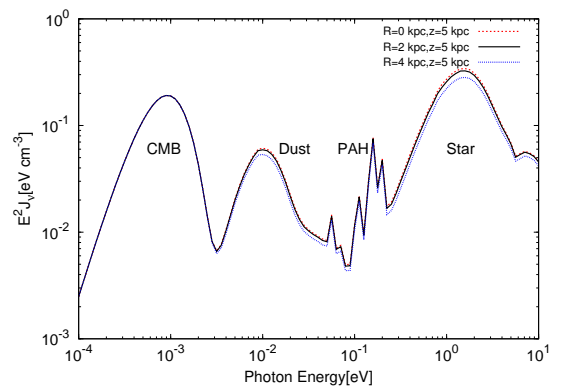


FIG. 2.— Interstellar radiation field from GALPROP v54. We adopt the black solid line ($R = 2$ kpc, $z = 5$ kpc) as a representative field of the whole region.

The electron injection into the stochastic acceleration is also an unknown process similarly to that in the shock acceleration. The background cosmic-rays distributed in the upstream region in advance may be re-accelerated by the turbulence (see §5). Here, we simply assume the injection term with the same power-law temporal evolution as D :

$$Q_{\text{inj}}(p, t) = Q_0 \delta(p - p_0) \left(1 + \frac{t}{t_0}\right)^{-\alpha}. \quad (5)$$

An injection rate proportional to the inverse of the acceleration timescale may be reasonable as a first-step assumption. The injection energies are taken as $cp_0 = 10^8$ eV and 10^{10} eV for electrons and protons, respectively. Though the actual injection energy may be lower than our assumptions, note that the parameter Q_0 is related to the electron flux at $p = p_0$ in momentum space for electrons accelerated from lower momenta.

While MS11 counted electrons only in the DRs, the escaped particles should contribute to the emissions of the FBs as well. The escaped particles cool without the acceleration effect. We calculate the evolution of the escaped particles as

$$\frac{\partial n_{\text{esc}}}{\partial t} + \frac{\partial}{\partial p} \left(\frac{dp}{dt} n_{\text{esc}} \right) - Q_{\text{inj}}^{\text{esc}} = 0, \quad (6)$$

¹ <http://galprop.stanford.edu/>

where the injection term for the escaped particles $Q_{\text{inj}}^{\text{esc}}$ is equal to n/t_{esc} . For simplicity, we neglect the reentry of the escaped particles into the DRs.

We simultaneously solve equations (1) and (6). In our method, the obtained temporal evolutions for $n(t)$ and $n_{\text{esc}}(t)$ are interpreted as the spatial distributions of $n(x)$ and $n_{\text{esc}}(x)$ at the present moment. The time t and the distance from the shock front x are connected as $x = v_{\text{sh}}t$ (see Figure 1), then the radial position is written as $R = R_{\text{sh}} - x$, where R_{sh} is the radius of the shock front. Hereafter, we adopt a constant value of $v_{\text{sh}} = 250 \text{ km s}^{-1}$, which is consistent with the X-ray observations of the FBs (Tahara et al. 2015). Of course, the expansion speed of the FBs may be not constant and depend on the energy injection history and the density profile (e.g. Guo & Mathews 2012; Zubovas & Nayakshin 2012; Baumgartner & Breitschwerdt 2013; Fujita, Ohira & Yamazaki 2013; Lacki 2014). The deceleration/acceleration of the shock front makes our model complicated, and forces us to (at least) a 1D calculation rather than a one-zone approximation. To simplify our model, we assume that the shock speed has not changed drastically in the last period of a few megayears. This assumption is consistent with almost constant shock velocity at the last stage in the prompt energy injection model of Fujita, Ohira & Yamazaki (2014) based on the galactic halo profile in Guo & Mathews (2012). Even in the long energy injection model of Crocker et al. (2015), the shock velocity is almost constant after a few megayears from the onset of the energy injection. The almost constant electron density at a scale of 1–2 kpc behind the shock in the simulations of ~ 10 Myr activity of the galactic nucleus by Mou et al. (2014) also supports our simple assumption indirectly.

We numerically calculate the spectral evolutions of n and n_{esc} as far as $x = 2 \text{ kpc}$ ($0 < t < 7.8 \text{ Myr}$). This provides us with the radial dependence of the emissivity. Assuming spherical symmetry, we calculate the surface brightness by integrating the emissivity along the line of sight. We neglect the emissions from the region inside $R_{\text{sh}} - 2 \text{ kpc}$. The emission processes we consider are synchrotron, IC, and pion decay ($\pi^0 \rightarrow 2\gamma$) arising from a pp collision. The numerical method to calculate such emission spectra is the same as that in Asano & Mészáros (2012) and Murase et al. (2012).

If the plasmas in the FBs have temperatures of $\sim 0.3 \text{ keV}$ (Tahara et al. 2015), density $\sim 10^{-3} \text{ cm}^{-3}$, and magnetic field $\sim 4\mu\text{G}$, both the Alfvén speed and sound speed are on the order of 10^7 cm s^{-1} . So we adopt $\beta_{\text{W}} = 5.0 \times 10^{-4}$ hereafter. Even if β_{W} is different, we can obtain similar results by scaling the parameters D and L .

3. LEPTONIC MODELS

The phenomenological model parameters are B_0 , D_0 , α , Q_0 , L , and R_{sh} . The value D_0 adjusts the acceleration efficiency, Q_0 normalizes the flux level, L controls the timescales t_0 and t_{esc} , and R_{sh} is the actual shock front that may be displaced from the observed edge of the FBs. For leptonic models, we show three models in which the temporal decay indices are assumed as $\alpha = 1$. The other parameters are summarized in Table 1.

As a test case, we adopt the exact same values and evo-

lutions for D_{pp} and t_{esc} as those in MS11, in which fast magnetosonic waves injected at a relatively large scale of 2 kpc are responsible for the acceleration. While MS11 assumed the steady-state solution for each radius, we numerically follow the temporal evolutions of the electron energy distribution with the evolving D_{pp} and constant injection rate Q_{inj} .² Although the obtained results are different from the steady-state solutions, we omit to show those results in this paper. The parameters for model NoE, whose results will be shown in the next subsection, are adjusted to yield a similar D_{pp} evolution to the model of MS11.³ Consequently, the obtained spectra for electrons and gamma-rays also become similar to those in MS11.

3.1. No Escape Model

In model NoE, the filling factor of the DRs is simply assumed to be unity. Namely, the turbulence is distributed over the whole FBs. In this case, there is no effect of electron escape. Once electrons are injected, they are continuously affected by the turbulence.

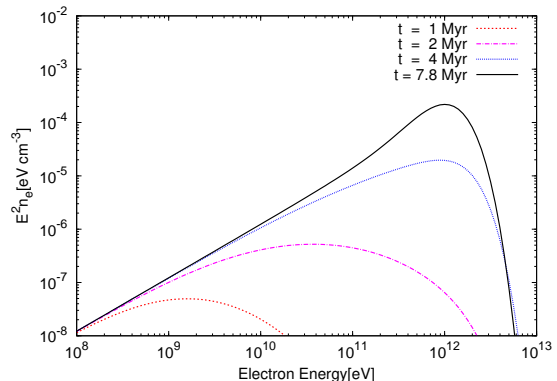


FIG. 3.— Evolution of the electron spectrum for the NoE model.

In Figure 3, we plot the evolution of the electron spectrum. Each time in the figure (1, 2, 4, 7.8 Myr) corresponds to the distance from the shock front (0.26, 0.51, 1.0, 2.0 kpc, respectively). Apparently, the maximum energy of electrons gradually grows with time. The energy distribution is not the steady-state solution, since the initial acceleration timescale $p^2/D_{pp}(0) = 3/(2\beta_{\text{W}}^2 D_0) \simeq 1.3 \text{ Myr}$, which is independent of electron energy, and the cooling timescale

$$t_{\text{cool}} = \frac{3m_e c}{4\sigma_{\text{T}} \gamma U_{\text{ph}}} \simeq 340 \left(\frac{E}{10^9 \text{ eV}} \right)^{-1} \left(\frac{U_{\text{ph}}}{1.5 \times 10^{-12} \text{ erg cm}^{-3}} \right)^{-1} \text{ Myr}, \quad (7)$$

are long enough compared to the elapsed time. The electron spectrum becomes harder with increasing time. The cooling effect is not so sufficient that the energy density of electrons increases with time or x . At later stages (see the line of 7.8 Myr), the spectrum becomes similar to the

² MS11 did not explicitly declare the injection rate profile.

³ The evolution of D_{pp} is not a power-law form of x in MS11.

TABLE 1
PARAMETERS FOR LEPTONIC MODELS

Model	L (pc)	D_0 (s $^{-1}$)	Q_0 (cm $^{-3}$ s $^{-1}$)	R_{sh} (kpc)	E_{tot} (erg)
NoE (No Escape)	1500 ^a	1.5×10^{-7}	5.9×10^{-30}	4.4	1.1×10^{53}
MiE (Mild Escape)	180	4.0×10^{-7}	4.2×10^{-29}	3.6	2.6×10^{53}
EfE (Efficient Escape)	10	4.0×10^{-6}	7.4×10^{-27}	3.0	2.0×10^{54}

^a In model NoE, we neglect the escape effect, so L provides the timescale t_0 only.

steady solution, in which a spectral bump at $\sim 10^{12}$ eV is formed by the balance of the acceleration and cooling.

As we have mentioned, even if we adopt the same model as MS11 with the escape effect, the time-dependent calculation yields a similar evolution of n to that in Figure 3. This is an opposite manner of the spatial dependence of the electron spectrum in MS11; the steady solution in MS11 shows a hard-to-soft distribution from the shock front to the downstream. Note that the escape timescale in MS11 is ~ 100 –400 Myr so that the escape effect can be neglected. The steady-state solutions may not be appropriate to describe the electron energy distribution.

In our model, the electron spectrum is maintained hard during the calculation, because the escape effect is neglected. As a result, the gamma-ray spectrum below 1 GeV becomes too hard, as shown in Figure 4. Another problem is that the surface brightness monotonically increases as the radius approaches to the center. As shown in Figure 5, the inner boundary at $x = 2$ kpc is reflected on the surface brightness as a sharp peak. Unless such an artificial cavity exists, the surface brightness profile should have a peak at the center in this model. The nearly homogeneous surface brightness is difficult to be reproduced with this model.

The photon spectra and surface brightness obtained by the time-dependent calculation with the same model as MS11 are also similar to Figures 4 and 5. In order to soften the spectrum, especially for the inner region, the escape effect should be incorporated.

3.2. Mild Escape Model

To soften the electron and photon spectra, the escape effect should be involved. In the MiE model, we take into account the escape effect with the initial timescale of $t_{\text{esc}} = 3L^2 D_0 / c^2 = 13$ Myr, which is much longer than $t_0 = L/v_{\text{sh}} = 0.7$ Myr and the acceleration timescale, 0.48 Myr. As time passes, the escape timescale shortens, while the acceleration timescale grows. In Figure 6, we show the evolution of the total electron spectrum (namely, $n + n_{\text{esc}}$). At $t = 2$ Myr, the escape effect is still negligible, so the electrons in the DRs still dominate for the entire energy region. Even at $t = 4$ Myr, the peak energy region ($\sim 10^{12}$ eV) is dominated by the electrons in the acceleration process. However, in the low-energy power-law-like region (below $\sim 10^{11}$ eV), the escaped electron density is comparable to that in the DRs. At the last stage ($t = 7.8$ Myr), the IC cooling makes a spectral peak for the escaped electrons at $\sim 10^{11}$ eV, while the highest energy region ($\sim 10^{12}$ eV) is still dominated by the electrons in the DRs.

The softening of the electron spectrum due to the IC cooling and escape effects understandably produces a softer gamma-ray spectrum than the NoE model spec-

trum. As shown in Figure 7, the resultant spectrum agrees well with the observation above 10^8 eV. The surface brightness profiles also agree with the observed properties: sharp rise at the edge and flat profile inside (see Figure 8).

Even with the best-fit parameters for the MiE model, the radio intensity is far below the observed data of the WMAP haze (see Figure 7). While we have assumed $B_0 = 4\mu\text{G}$, a stronger magnetic field such as 10–20 μG may be required as shown in MS11 (see also, e.g. Ackermann et al. 2014) to reconcile the radio intensity. However, the magnetic field model in Orlando & Strong (2013), which agrees with all-sky total intensity and polarization maps, may not allow such a high field.

3.3. Efficient Escape Model

In this subsection, we try to find a model that agrees with not only the gamma-ray spectrum but also the WMAP haze. The electron spectrum should be softer than that in the MiE model. We adopt a very small size for L in the EfE model, so the escape effect will be more prominent. To accelerate electrons as far as 10^{12} eV before escaping from the DRs, a higher value for D_0 is adopted here.

The initial timescales are $t_0 = 0.039$ Myr, $t_{\text{acc}} = 0.048$ Myr, and $t_{\text{esc}} = 0.40$ Myr. At $t = 0.086$ Myr, the acceleration and escape timescales become comparable as ~ 0.13 Myr. At $t = 0.2$ Myr (see Figure 9), most electrons above 10^{10} eV are still in the DRs. However, the escaped electrons become dominant in the later phase ($t > 0.3$ Myr). Then, the acceleration efficiency quickly damps. The inefficiency of the acceleration in the later phase is due to not only the escape effect but also the growth of the acceleration timescale. The non-steady electron spectrum in the early acceleration stage is therefore frozen after the decay of the acceleration efficiency. This leads to the soft electron spectrum. Owing to the fast decay of the acceleration efficiency, the electrons injected later almost remain at the injection energy so that an artificial spectral peak is seen at 10^8 eV. The spectral cutoff due to the IC cooling ($t_{\text{cool}} = 0.34(E/10^{12} \text{ eV})^{-1}$ Myr) is clearly seen in the electron spectra for $t \geq 1$ Myr in Figure 9.

The resultant photon spectrum becomes so soft that the radio intensity of the WMAP haze is also reproduced as seen in Figure 10. The model flux at 10^8 eV is slightly higher than the observation, but may still be within the systematic uncertainty. The surface brightness profiles do not seem to deviate from the observed profiles very much (see Figure 11), but the short acceleration period makes a slight limb brightening. In this model, the initial acceleration timescale is much shorter than the previous models. Therefore, the positions of the shock front and the FB edge are identical in this case.

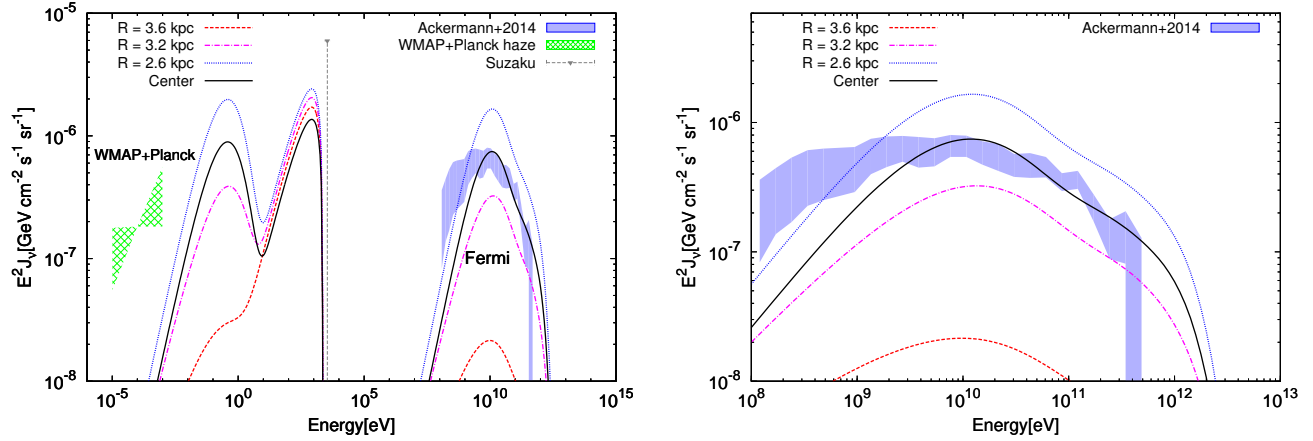


FIG. 4.— Broadband photon spectra of the NoE model (left) and their zoom-in display in the gamma-ray band (right). The thermal bremsstrahlung spectrum in the X-ray band is plotted assuming a proton density of 10^{-3} cm^{-3} and electron temperature of keV for reference. The observed data are taken from Ackermann et al. (2014) for the Fermi-LAT data, and Kataoka et al. (2013) for the WMAP+Planck data and the X-ray upper limit.

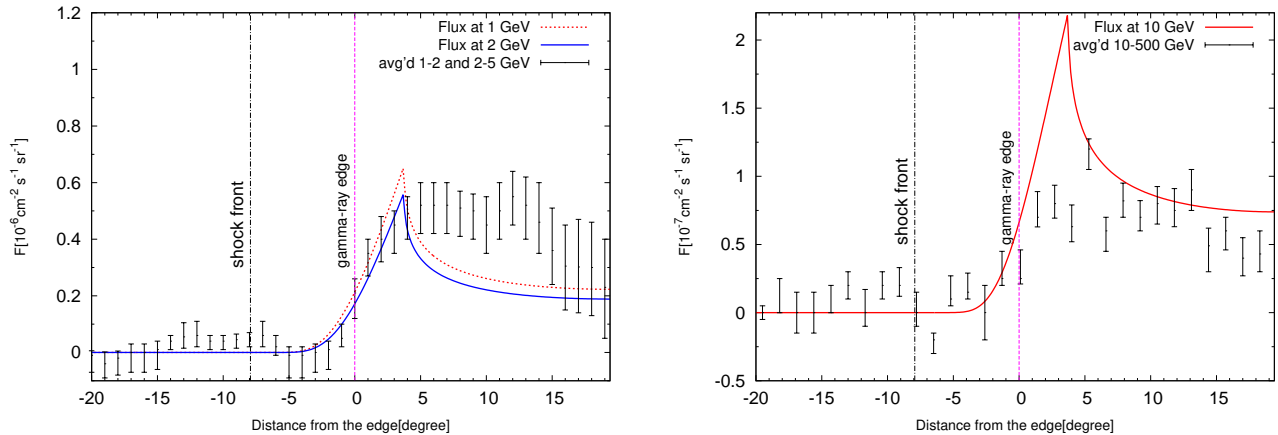


FIG. 5.— Gamma-ray intensity of the NoE model as a function of distance from the gamma-ray edge for 1 GeV (dotted) and 2 GeV (solid) profiles (left panel) with the data from Su et al. (2010), and for 10 GeV (solid) profile (right panel) with the data from Ackermann et al. (2014).

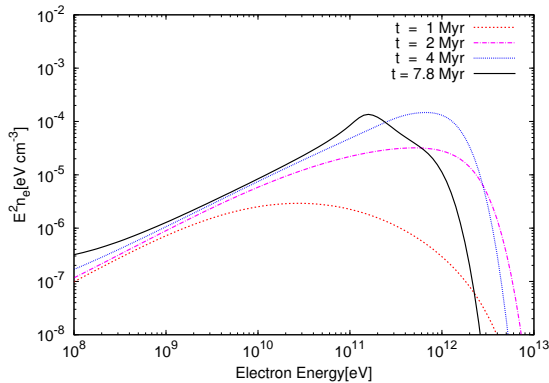


FIG. 6.— Evolution of the total electron spectrum for the MiE model.

4. HADRONIC MODELS

A hadronic model with stochastic acceleration is also possible in theory. The acceleration mechanism is common for electrons and protons other than the injection

process. The accelerated protons should obviously exist in the situation we have considered in this paper. High-energy protons collide with the thermal protons, and produce pions that decay into gamma-rays, which may be responsible for the gamma-ray emission in the FBs. Similarly to the leptonic models, we test three models as summarized in Table 2. The radiative cooling effect is neglected so that the difference between protons in the DRs and escaped protons is the acceleration process only. We adopt $\alpha = 1$ again. The background density of protons as the targets for pp -collision is assumed to be uniform with 10^{-3} cm^{-3} .

In Figure 12, we plot the gamma-ray spectra at the center ($l = 0^\circ$) for the three models. As the escape effect becomes efficient, the photon spectrum softens. Although the hadronic models can generate a photon spectrum similar to the observed one, the required total energy becomes much larger than those in the leptonic models (compare E_{tot} in Tables 1 and 2, where total energies integrated over the whole volume are shown). In such cases, electrons should be accelerated as well. Even if the electron energy fraction to the proton energy is plausi-

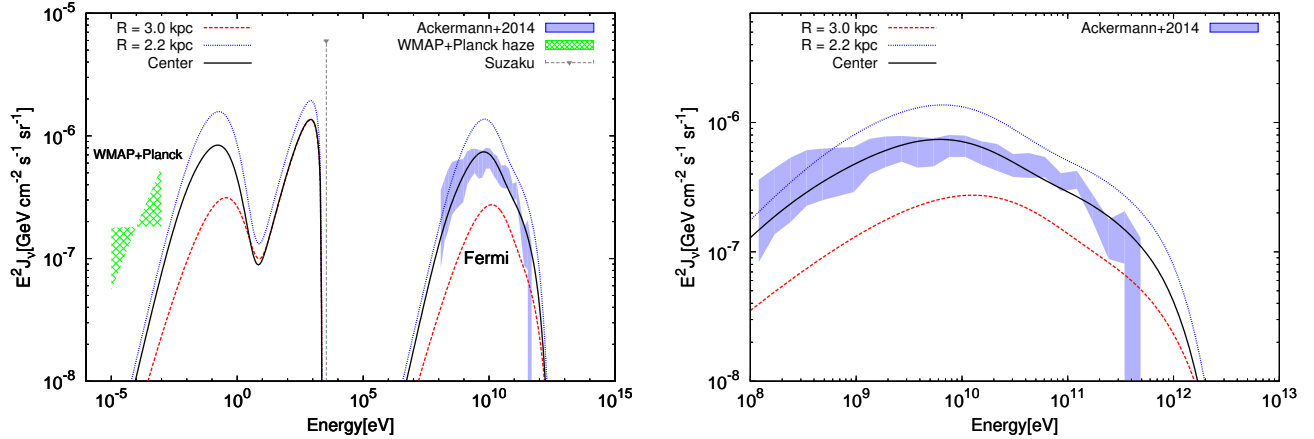


FIG. 7.— Same as Fig. 4 but for the MiE model.

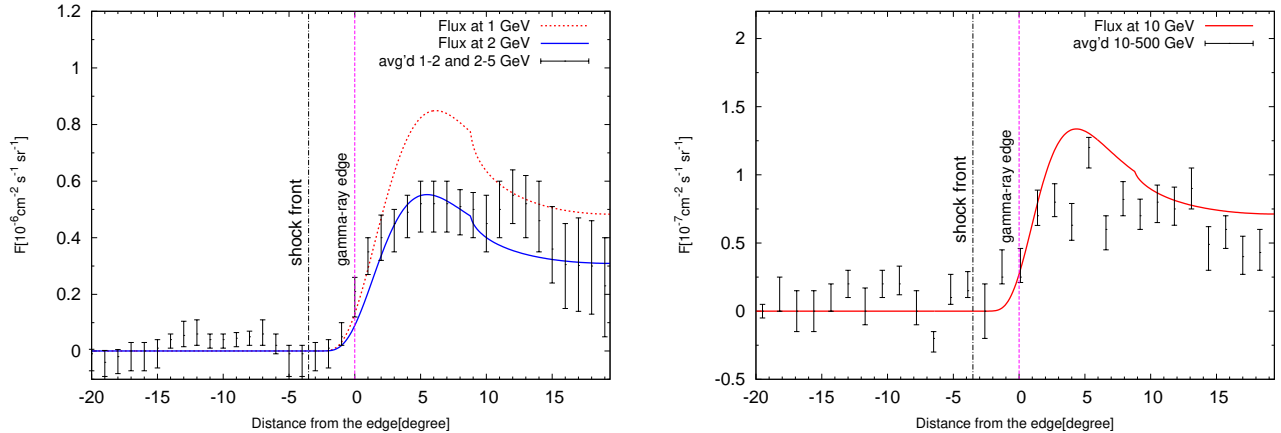


FIG. 8.— Same as Fig. 5 but for the MiE model.

TABLE 2
PARAMETERS FOR HADRONIC MODELS

Model	L (pc)	D_0 (s^{-1})	Q_0 ($cm^{-3} s^{-1}$)	R_{sh} (kpc)	E_{tot} (erg)
pNoE (No Escape)	1500 ^a	1.0×10^{-7}	1.1×10^{-25}	4.4	1.4×10^{57}
pMiE (Mild Escape)	180	1.4×10^{-7}	1.8×10^{-25}	3.6	1.4×10^{57}
pEfE (Efficient Escape)	10	1.2×10^{-6}	3.9×10^{-25}	3.0	2.2×10^{57}

^a In model pNoE, we neglect the escape effect, so L provides the timescale t_0 only.

bly theoretical minimum-value, m_e/m_p , the gamma-ray emission would be dominated by IC emission by electrons. Therefore, the hadronic models with the stochastic acceleration seem contrived. Furthermore, the synchrotron flux from secondary electrons/positrons is too dim to reconcile the WMAP haze.

5. SUMMARY AND DISCUSSION

In our model, the shock fronts are propagating outward with a low Mach number so that the direct particle acceleration by the shock waves may be inefficient. Some kind of turbulence is induced just behind the shock front, and gradually decays with time. Particles are accelerated via scattering with the turbulence. Considering the efficiency of gamma-ray emission, the leptonic model is more

likely than the hadronic model for stochastic acceleration models. The adequate acceleration timescale is initially 0.05–0.5 Myr. Our results show that the steady solutions for the Fokker–Planck equation are not adequate in the FBs. The time interval in which the maximum electron energy reaches 10^{12} eV is not negligible compared to the bubble expansion timescale. We also show that the escape effect may be indispensable to reproduce the gamma-ray spectrum especially below 1 GeV. If electrons are continuously accelerated, the electron spectrum becomes too hard to agree with the observed gamma-ray spectrum. For the escaped electrons, the termination of the acceleration and succeeding cooling effect generate a soft spectrum. The combination of the two electron species, those in the acceleration region and those hav-

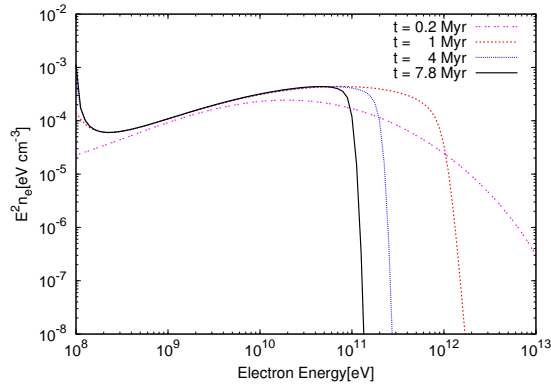


FIG. 9.— Evolution of the total electron spectrum for the EFe model.

ing escaped, can produce the best-fit model for the FBs. In addition, the long-term evolution of the electron spectrum, which is regulated by the finite timescales of t_0 , t_{acc} , t_{esc} , and t_{cool} , is favorable for the almost constant surface brightness. Moreover, assuming a very short t_{esc} , we can reproduce the spectra of both the FBs and WMAP haze with the reasonable magnetic field.

While we cannot determine the model parameters uniquely, our results modestly constrain a parameter range. If the turbulence decay is much faster than our models, the initial acceleration efficiency should be high. In such cases, the particle acceleration and gamma-ray emission occur near the shock front only. This leads to significant limb brightening in the surface brightness profile as seen in the synchrotron emission from shock-accelerated electrons in supernova remnants. So a too small t_0 (or equivalently L) or $\alpha = 2$ seem unfavorable.

In order to make electrons escape from the acceleration process in a certain timescale, we assume a finite

size of the DR. An inhomogeneity in the upstream region is required with a significant filling factor. The region size L required in our model is comparable to the size of the inhomogeneity expected from several studies, such as the numerical simulations of the interaction between a galactic wind and hot halo gas (Melioli et al. 2013; Sharma et al. 2014) or formation of galactic fountain clouds (Fraternali et al. 2015). This coincidence encourages us assuming such localized acceleration regions.

The average electron density at $x = 2$ kpc obtained from Table 1 is $2.3 \times 10^{-15} \text{ cm}^{-3}$ in the MiE model. Those electrons may be injected from the background plasma. Though the cosmic-ray electron density in the halo is highly uncertain (e.g. Orlando & Strong 2013), that can be 1–50% of the local density, $\sim 10^{-13} \text{ cm}^{-3}$ (Ackermann et al. 2010). Considering the uncertainty of the filling factor, the re-acceleration of the background cosmic-ray electrons seems a promising model for the electron injection mechanism.

The spatial diffusion coefficient inside the Galactic disk is $5 \times 10^{28} \text{ cm}^2 \text{ s}^{-1}$ at 3–4 GeV (Ackermann et al. 2012). If a Kolmogorov-like turbulence dominates ($D_{xx} \propto p^{1/3}$), the diffusion coefficient at 10^{12} eV becomes $\sim 10^{29} \text{ cm}^2 \text{ s}^{-1}$. On the other hand, our model parameters infer $D_{xx} = 7.5 \times 10^{25} - 7.5 \times 10^{26} \text{ cm}^2 \text{ s}^{-1}$ independently of the particles' energy. As a matter of course, the mean free path in the DRs ($10^{-3} - 10^{-2} \text{ pc}$) is much shorter than the local value near the Sun ($\sim \text{pc}$ at 10^{12} eV), but much longer than the Larmor radius.

We thank the anonymous referee for a careful review and valuable comments. We appreciate Y. Fujita and Y. Ohira for helpful discussion. This work is partially supported by the Grant-in-Aid for Scientific Research, No. 25400227 from the MEXT of Japan (KA).

REFERENCES

- Ackermann, M., et al. 2010, *Phys. Rev. D*, 82, 092004
 Ackermann, M., et al. 2012, *ApJ*, 750, 3
 Ackermann, M., et al. 2014, *ApJ*, 793, 64
 Asano, K., & Hayashida, M. 2015, *ApJ*, 808, L18
 Asano, K., & Mészáros, P. 2012, *ApJ*, 757, 115
 Asano, K., Takahara, F., Kusunose, M., Toma, K., & Kakuwa, J. 2014, *ApJ*, 780, 64
 Asano, K., & Terasawa, T. 2009, *ApJ*, 705, 1714
 Baumgartner, V., & Breitschwerdt, D. 2013, *A&A*, 557, A140
 Blandford, R., & Eichler, D. 1987, *PhR*, 154, 1
 Brandenburg, A., Kahniashvili, T., & Tevzadze, A. G. 2015, *Phys. Rev. Lett.*, 114, 075001
 Cheng, K. S., Chernyshov, D. O., Dogiel, V. A., & Ko, C. M. 2014, *ApJ*, 790, 23
 Cheng, K. S., Chernyshov, D. O., Dogiel, V. A., & Ko, C. M. 2015a, *ApJ*, 799, 112
 Cheng, K. S., Chernyshov, D. O., Dogiel, V. A., & Ko, C. M. 2015b, *ApJ*, 804, 135
 Cheng, K. S., Chernyshov, D. O., Dogiel, V. A., Ko, C. M., & Ip, W. H. 2011, *ApJ*, 731, L17
 Cho, J., & Lazarian, A. 2006, *ApJ*, 638, 811
 Christensson, M., Hindmarsh, M., & Brandenburg, A. 2001, *Phys. Rev. E*, 64, 056405
 Crocker, R. M. 2012, *MNRAS*, 423, 3512
 Crocker, R. M., & Aharonian, F. 2011, *Phys. Rev. Lett.*, 106, 101102
 Crocker, R. M., Bicknell, G. V., Taylor, A. M., & Carretti, E. 2015, *ApJ*, 808, 107
 Dobler, G., & Finkbeiner, D. P. 2008, *ApJ*, 680, 1222
 Fan, Z., Liu, S., & Fryer, C. L. 2010, *MNRAS*, 406, 1337
 Finkbeiner, D. P. 2004, *ApJ*, 614, 186
 Fraternali, F., Marasco, A., Armillotta, L., & Marinacci F. 2015, *MNRAS*, 447, L70
 Fujita, Y., Ohira, Y., & Yamazaki, R. 2013, *ApJ*, 775, L20
 Fujita, Y., Ohira, Y., & Yamazaki, R. 2014, *ApJ*, 789, 67
 Guo, F., & Mathews, W. G. 2012, *ApJ*, 756, 181
 Hardcastle, M. J., Cheung, C. C., Feain, I. J., & Stawarz, L. 2009, *MNRAS*, 393, 1041
 Inoue, T., Yamazaki, R., & Inutsuka, S. 2009, *ApJ*, 695, 825
 Kakuwa, J., Toma, K., Asano, K., Kusunose, M., & Takahara, F. 2015, *MNRAS*, 449, 551
 Kataoka, J., et al. 2013, *ApJ*, 779, 57
 Lacki, B. C. 2014, *MNRAS*, 444, L39
 Liu, S., Melia, F., Petrosian, V., & Fatuzzo, M. 2006, *ApJ*, 647, 1099
 Lynn, J. W., Quataert, E., Chandran, B. D. G., & Parrish, I. J. 2014, *ApJ*, 791, 71
 Melioli, C., de Gouveia Dal Pino, E. M., & Geraissate, F. G. 2013, *MNRAS*, 430, 3235
 Mertsch, P., & Sarkar, S. 2011, *Phys. Rev. Lett.*, 107, 091101 (MS11)
 Mou, G., Yuan, F., Bu, D., Sun, M., & Su, M. 2014, *ApJ*, 790, 109
 Mueller, E., Fryxell, B., & Arnett, D. 1991, *A&A*, 251, 505
 Murase, K., Asano, K., Terasawa, T., & Mészáros, P. 2012, *ApJ*, 746, 164
 Ohira, Y., Murase, K., & Yamazaki, R. 2011, *MNRAS*, 410, 1577
 Orlando, E., & Strong, A. 2013, *MNRAS*, 436, 2127

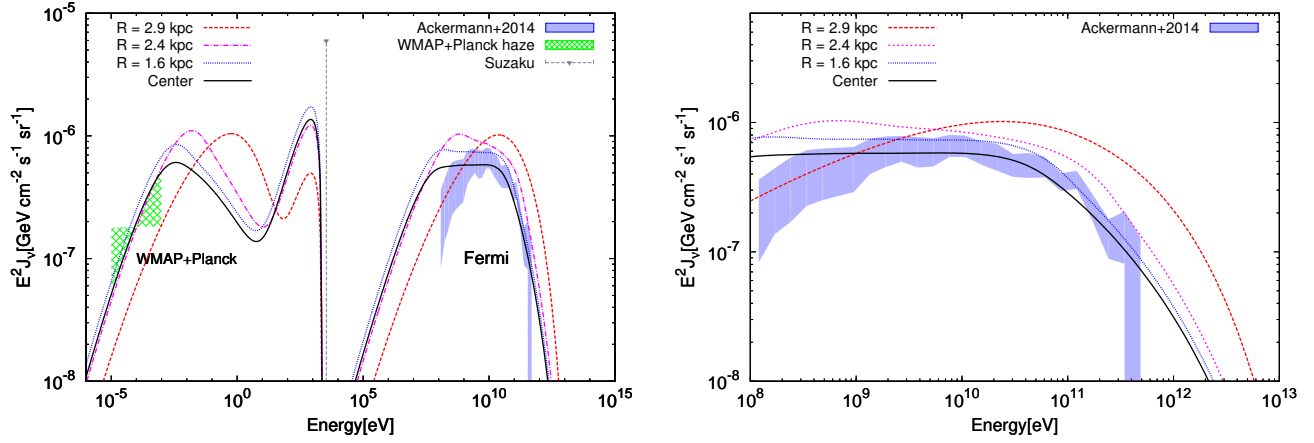


FIG. 10.— Same as Fig. 4 but for the Efe model.

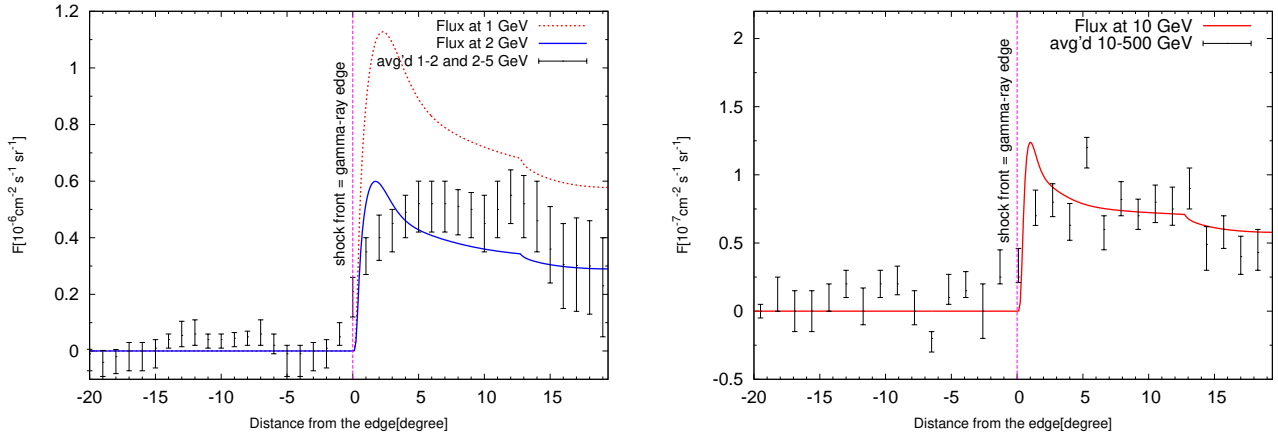


FIG. 11.— Same as Fig. 5 but for the Efe model.

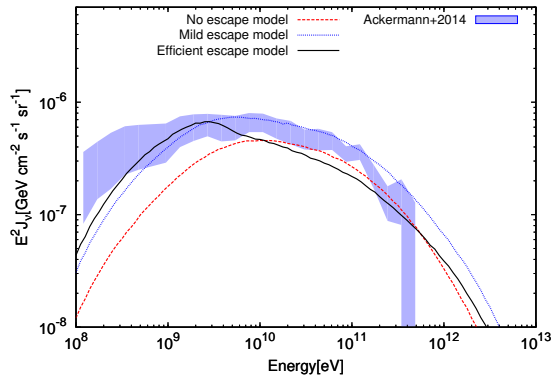


FIG. 12.— Photon spectra at the center of the FBs for three hadronic models. The observed data are taken from Ackermann et al. (2014).

Porter, T. A. & Strong, A. W. 2005, Proc. 29th Int. Cosmic Ray Conf., Pune, 4, 77
 Ptuskin, V. S. 1988, Soviet Astron. Lett., 14, 255
 Sharma, M., Nath, B. B., Chattopadhyay, I., & Shchekinov Y. 2014, MNRAS, 441, 431
 Stawarz, L., & Petrosian, V. 2008, ApJ, 681, 1725
 Su, M., Slatyer, T. R., & Finkbeiner, D. P. 2010, ApJ, 724, 1044
 Su, M., & Finkbeiner, D. P. 2012, ApJ, 753, 61
 Tahara, M., Kataoka, J., Takeuchi, Y., et al. 2015, ApJ, 802, 91
 Vladimirov, A. E., Digel, S. W., Jóhannesson, G., et al. 2011, Computer Physics Communications, 182, 1156
 Yang, C., & Liu, S. 2013, ApJ, 773, 138
 Yang, H.-Y. K., Ruszkowski, M., Ricker, P.M., Zweibel, E., & Lee, D. 2012, ApJ, 761, 185
 Yang, R., Aharonian, F., & Crocker, R. M. 2014, A&A, 567, A19
 Zubovas, K., King, A. R., & Nayakshin, S. 2011, MNRAS, 415, L21
 Zubovas, K., & Nayakshin, S. 2012, MNRAS, 424, 666